Agricultural and Forest Meteorology 249 (2018) 163–175

Contents lists available at ScienceDirect

Agricultural and Forest Meteorology

journal homepage: www.elsevier.com/locate/agrformet

Contrasting responses of grassland water and carbon exchanges to climate change between Tibetan Plateau and Inner Mongolia

Dan Liu[a], Yue Li[b], Tao Wang[a,c,*], Philippe Peylin[d], Natasha MacBean[d], Philippe Ciais[d], Gensuo Jia[e], Mingguo Ma[f,g], Yaoming Ma[a,c], Miaogen Shen[a,c], Xianzhou Zhang[h], Shilong Piao[a,b,c]

[a] Key Laboratory of Alpine Ecology and Biodiversity, Institute of Tibetan Plateau Research, Chinese Academy of Sciences, Beijing 100101, China
[b] Sino-French Institute for Earth System Science, College of Urban and Environmental Sciences, Peking University, Beijing 100871, China
[c] CAS Center for Excellence in Tibetan Plateau Earth Sciences, Chinese Academy of Sciences, Beijing 100101, China
[d] Laboratoire des Sciences du Climat et de l'Environnement, LSCE/IPSL, CEA-CNRS-UVSQ, Université Paris-Saclay, F-91191 Gif-sur-Yvette, France
[e] TEA, Institute of Atmospheric Physics, Chinese Academy of Sciences, Beijing, 100029, China
[f] Key Laboratory of Remote Sensing of Gansu Province, Cold and Arid Regions Environmental and Engineering Research Institute, Chinese Academy of Sciences, No. 320 Donggang West Road, Lanzhou 730000, China
[g] School of Geographical Sciences, Southwest University, No. 2 Tiansheng Road, Chongqing 400715, China
[h] Key Laboratory of Ecosystem Network Observation and Modeling, Lhasa Plateau Ecological Research Station, Institute of Geographic Sciences and Natural Resources Research, Chinese Academy of Sciences, Beijing 100101, China

ARTICLE INFO

Keywords:
Grassland
Climate change
Tibetan Plateau
Inner Mongolia
ORCHIDEE model

ABSTRACT

The grassland ecosystems in Tibetan Plateau (TP) and Inner Mongolia (IM) of China play important roles in climate change mitigation and food and livestock production. These two regions have increasingly experienced higher temperatures and changing precipitation regimes over the past three decades. However, it remains uncertain to what extent rising temperature and varying precipitation regulate the water and carbon fluxes across alpine (TP) and temperate (IM) grasslands. Here, we first optimize a process-based model of carbon and water fluxes using eddy-covariance data (three sites in TP and six sites in IM), and analyze the simulated carbon and water fluxes based upon the optimized model exposed to a range of annual temperature and precipitation anomalies. We found that the changes in net ecosystem-atmosphere carbon exchange (NEE) of TP grassland are relatively small because the ecosystem respiration (R_e) and the gross primary productivity (GPP) increase at comparable rate with warming across multiple sites (R_e: 22.1 ± 21.4 g C m^{-2} $year^{-1}$ $°C^{-1}$, GPP: 22.43 ± 36.41 g C m^{-2} $year^{-1}$ $°C^{-1}$), which is due to the possibility that grasslands cannot respire more than the available supply of photosynthesis. The NEE of IM grassland increases (more carbon loss from ecosystem) with warming, which is mainly because GPP decreases faster than R_e under warm-induced reduction in moisture availability, and the sensitivity of R_e to warming (1.17 ± 3.56 g C m^{-2} $year^{-1}$ $°C^{-1}$) is much smaller than that of GPP (15.53 ± 15.91 g C m^{-2} $year^{-1}$ $°C^{-1}$). These results indicate that water is the major limiting factor in IM grasslands, but not in TP grasslands. In contrast to warming, we found an asymmetric response of water and carbon fluxes to drying and wetting in TP grasslands (i.e. a large decrease under the drying condition and a small increase under the wetting condition) but almost a linear response in IM grasslands. We therefore highlight that the underlying processes regulating the responses of water and carbon cycles to warming are fundamentally different between TP and IM grasslands, with the moisture being the major limiting factor in IM while grasslands in TP are much more limited by thermal conditions. Our results also imply that warming would significantly stimulate the net ecosystem carbon loss to atmosphere but not significantly enhance ET in IM grasslands, which may provide a positive feedback to accelerate climate change. Inversely, warming could not significantly affect the ecosystem carbon exchange but significantly enhance ET in TP grasslands, which may provide a negative feedback to mitigate climate change in alpine grasslands.

1. Introduction

Grasslands in China are mainly distributed in Tibetan Plateau and Inner Mongolia that harbor the largest portion of alpine (1.5×10^6 km^2) (Zhang et al., 2014) and temperate grasslands (7.8×10^5 km^2) (Briske et al., 2015), respectively. Both Tibetan

* Corresponding author at: Key Laboratory of Alpine Ecology and Biodiversity, Institute of Tibetan Plateau Research, Chinese Academy of Sciences, Beijing 100085, China.
E-mail address: twang@itpcas.ac.cn (T. Wang).

https://doi.org/10.1016/j.agrformet.2017.11.034
Received 1 February 2017; Received in revised form 1 October 2017; Accepted 29 November 2017
Available online 12 December 2017
0168-1923/ © 2017 Elsevier B.V. All rights reserved.

Plateau and Inner Mongolia have experienced significant climate change over the past few decades (Gong et al., 2004; IPCC, 2013). For example, air temperature in Tibetan Plateau (0.16 °C decade^{-1}) and Inner Mongolia (0.35 °C decade^{-1}) increased significantly in the past five decades, with the increasing rate higher than that over the Northern Hemisphere (0.05 °C decade^{-1}) (Liu and Chen, 2000; Wang et al., 2008a,b; Lu et al., 2009). In contrast, the precipitation shows a slightly decreasing trend in Inner Mongolia (Gong et al., 2004), but a mixed trend over Tibetan Plateau, with a decrease in its southern and eastern regions, and an increase in its central and western regions (Tong and Zhang, 2003; Yang, 2017). These changes in temperature and precipitation could profoundly affect terrestrial carbon and water cycles, having the potential to provide the feedback to climate change.

Although historical climate change is widely documented to significantly affect grassland carbon and water fluxes in these regions (Niu et al., 2008a,b; Piao et al., 2012; Li et al., 2017a), the processes underlying these responses are still not well understood or quantified. For example, previous studies of climate change impacts on carbon cycle are mostly focused on terrestrial production based on satellite-based proxies, with changes in precipitation having larger impacts than warming in Inner Mongolia and *vice versa* in part of Tibetan Plateau (Piao et al., 2006; Piao et al., 2012; Li et al., 2017a). But it remains unclear on the roles of the two terms (i.e. the length of CO_2 uptake denoting plant phenology, and maximum capacity of CO_2 uptake representing photosynthetic capacity) of ecosystem productivity (Xia et al., 2015; Wagle et al., 2015) in explaining the productivity responses to climate change. Moreover, Schwalm et al. (2010) analyzed global eddy-covariance (EC) flux data and found that terrestrial productivity is much more sensitive to drought event than respiration at global scale. But how terrestrial productivity and respiration respond to warming, altered precipitation and their interaction at the TP and IM grasslands is still not clear. Our current understandings of climate change impact on net grassland carbon balance (the net effect between carbon uptake through terrestrial production and carbon loss through respiration) and water balance are derived from manipulative experiments that mostly consider the effect of a single climate change factor with limited gradients [e.g. Niu et al., 2008a; Yang et al., 2016]. According to model projections, grasslands in Tibetan Plateau and Inner Mongolia could face a variety of future climate change scenarios, with various levels of precipitation changes superimposed onto different warming rates. In order to accurately predict regional carbon and water budgets, it is therefore imperative to understand the responses of carbon and water vapor fluxes to climate change including ecosystem exposure to a gradient of climate conditions and an interaction of climate change factors.

Resorting to climate change manipulative experiments is an ideal strategy for understanding the climate change impact on water and carbon cycles [e.g. Li et al., 2017a; Song et al., 2016; Chi et al., 2013; Wan et al., 2009]. But it is challenging and expensive in deploying manipulative experiments to understand how ecosystem responses to climate (temperature and precipitation) gradients and an interaction of different climate change factors. Land surface models would emerge as an optimal choice. But the direct application of the models in assessing future climate change impacts over grasslands of Tibetan Plateau and Inner Mongolia is not appropriate. On the one hand, the majority of current models are developed in regions outside of Tibetan Plateau and Inner Mongolia, with grassland related parameters either estimated from lab experiments or conditioned on specific location. On the other hand, grasses are always implemented in an aggregated form in the models through assuming that the parameters characterizing carbon and water fluxes are not dependent upon edaphic, climatic conditions and species composition. The prescription of the same model parameter set would definitely bias our understanding of the processes of ecosystem carbon and water fluxes on grasslands of Tibetan Plateau and Inner Mongolia that are respectively located in distinct climate regimes. It thus necessitates the well-constrained parameters over different grasslands based on the model-data fusion technique. Here using the data derived from the EC technique to optimize model parameters is preferred since this technique allows the continuous and non-destructive high frequency measurements of carbon and water fluxes (Baldocchi, 2003). Moreover, the derived carbon and water fluxes have been widely demonstrated to be valuable sources of the information for the development and optimization of land surface models in a wide range of ecosystems (Baldocchi et al., 2001; Peng et al., 2015; Li et al., 2017b; Kuppel et al., 2012, 2013, 2014; Lasslop et al., 2008; Yuan et al., 2007)

In this study, we conducted the analysis based on a series of model simulation experiments using the Organizing Carbon and Hydrology in Dynamics EcosystEms process based model. By comparing grasslands on Tibetan Plateau and Inner Mongolia we aim to gain insight into the mechanisms by which future changes in temperature, precipitation and their interaction may modify the function of these ecosystems. Because the model has not been calibrated for the Tibetan Plateau and Inner Mongolia grasslands and describes all C_3 grasslands with the same set of parameters, we first optimized the model parameters based on local EC flux data. Then we conduct idealized simulation experiments with a range of annual temperature and precipitation anomalies applied on current climate conditions to diagnose and discuss regionally different response of photosynthesis and water fluxes.

2. Data and methods

2.1. ORCHIDEE model

The ORCHIDEE model is a process-based ecosystem model with the ability to simulate the ecological processes (e.g. carbon cycle, vegetation dynamics) and land surface processes (e.g. the energy, water and momentum exchange between atmosphere and biosphere) (Krinner et al., 2005). In the ORCHIDEE model, the photosynthesis is described using the Farquhar equations (Farquhar et al., 1980; Collatz et al., 1992). The formulation of stomatal conductance is based on empirical correlations between conductance, photosynthetic rate, and relative humidity (Ball et al., 1987). The maximum rubisco-limited potential photosynthesis capacity is parameterized as a function of leaf age, soil water availability, and temperature (Ishida et al., 1999; Santaren et al., 2013). The dependence factor on soil water availability is a function of the water fraction available in the root zone and water stress parameter defining the opening of stomata occurs (Santaren et al., 2013). The temperature dependence of kinetic properties of Rubisco is described by the Arrhenius function (Yin and Struik, 2009). In this study we optimized the latest trunk version (Revision 3035) of ORCHIDEE to analyze the responses of carbon and water fluxes to altered temperature and precipitation on TP and IM grasslands.

2.2. Data assimilation system

The Organizing Carbon and Hydrology in Dynamics EcosystEms (ORCHIDEE) Data Assimilation System (ORCHIDAS, https://orchidas.lsce.ipsl.fr/index.php) was used in this study to conduct the parameter optimization. This model-data fusion framework is a combination of the ORCHIDEE model and a Bayesian inversion framework. Based on the ORCHIDEE model, the parameter optimization is conducted through a Bayesian inversion framework. Within this framework, the optimal parameters are determined based on the minimization of a quadratic cost function $J(x)$, which is the sum of two terms measuring the mismatch between the modeled and observed quantities and the mismatch between the estimated parameters and their prior values, with both terms being weighted by their uncertainties (Bacour et al., 2015):

$$J(x) = [(y - H(x))^T R^{-1}(y - H(x)) + (x - x_b)^T B^{-1}(x - x_b)]/2 \quad (1)$$

Where y is the observations, $H(x)$ is the model output, x represents the optimized parameter vector, x_b is the priori values of parameters, R and B are the error covariance matrices of observations and parameters,

respectively. To determine the optimal parameter set that minimizes $J(x)$, we obtained a "gradient-descent" algorithm (the L-BFGS-B quasi-Newton optimization algorithm) which is suitable for solving large nonlinear optimization problems that are subject to simple bounds on parameters. The L-BFGS-B algorithm explores the parameter spaces simultaneously along a gradient of the Eq. (1), and obtains an approximation of the second derivative of $J(x)$, that is updated during each iteration to define the size of the step at each iteration. The prior uncertainty of model parameters is defined as 40% of the physical range of parameter variations following Bacour et al., (2015). The prior observation error covariance matrix R includes errors from both measurements and model, and the observation error from EC measurements is often smaller than the model error (Kuppel et al., 2013). Here we set the observation error covariance matrix to be the root mean square error (RMSE) between EC observations and model simulations at each site following Kuppel et al., (2014). The errors on both the parameters and the observations are assumed to follow Gaussian distribution (Kuppel et al., 2014; Bacour et al., 2015). For the interest in improving model performance on both ecosystem carbon and water fluxes, we included daily NEE, GPP, and LE from EC measurements in the cost function.

To determine which parameters should be optimized, we performed a sensitivity analysis to identify the most influential parameters based on the Morris method (e.g. Lu et al., (2013)). Specifically, for each site, we selected the ten most influential PFT-specific parameters for NEE, GPP and LE respectively, and the parameters that are selected for either NEE, GPP or LE are then aggregated for this site. The selected parameters for each site are further aggregated to be the final selected parameter set for model parameter optimization (Table 1). Then we optimized these parameters at each site using the ORCHIDAS optimization scheme. The parameter values before and after parameterization are listed in Table 1 and Fig. S1.

2.3. Datasets and processing

The TP and IM are the two major regions where grasslands grow in China and have distinct climate features (Kato et al., 2004; Kato et al., 2006; Niu et al., 2011; Peng et al., 2013). The TP is mainly covered by alpine grasslands situating at an average altitude > 4000 m above the sea level, and is located between ~30 °N and 40 °N with high solar radiation during the growing season (Kato et al., 2006). The climate is cold, with annual temperature ranging from −15 °C to 5 °C (Shen et al., 2016). The IM grasslands growing on the Mongolian Plateau, with an average altitude around 1200 m and a typical arid or semiarid climate (Niu et al., 2008b). Along decreasing precipitation from east to west, grasslands on IM range from desert steppe on the west to meadow steppe on the east (Kang et al., 2007).

The grassland sites used in this study are listed in Table 2. All these sites have annual precipitation less than 500 mm year^{-1} (Fig. 1). Three sites are located on TP, with annual temperature ranging from −0.8 °C to 3.0 °C. Six sites are situated in central and eastern IM, with annual temperature varying between 1.5 °C and 7.4 °C. These sites cover major grassland types in China, including desert steppe (NaM), typical steppe (Du2, Xfs, Xi1, Xi2), degraded meadow (TNY) and alpine meadow in Tibet (HaM, DXG, ARG) (Table 2). More details about the characteristics of each site could be found in the references listed in Table 2.

We collected the half-hourly EC based flux data of the selected grassland sites from global FLUXNET dataset (http://www.fluxdata.org/), the ChinaFLUX (http://www.chinaflux.org/enn/index.aspx) and the AsiaFLUX (http://www.asiaflux.net). Data from the FLUXNET dataset are processed through standard procedures with detailed description of gap-filled methods and quality flag (Reichstein et al., 2005), while gaps exist in the data accessed from ChinaFLUX and AsiaFLUX dataset. To obtain continuous records, we filled the gaps in the measured NEE and LE time series, then partitioned NEE into GPP and ecosystem respiration (R_e) following the algorithms described in Reichstein et al. (2005) using the online EC gap-filling and flux-partitioning software (http://www.bgc-jena.mpg.de/~MDIwork/eddyproc/index.php). The half-hourly measured fluxes are highly auto-correlated, and fortunately this autocorrelation would rapidly decay as the time step increases, with the autocorrelation that can be negligible at the daily timescale (Lasslop et al., 2008). To avoid the influence of this data

Table 1
Descriptions of the parameters selected for optimization and parameter values before and after optimization for sites on Inner Mongolia (IM) and Tibetan Plateau (TP). The prior parameters are the default value with physical range in brackets of each parameter for the C_3 grass plant functional type (FTP). The post values represented here are mean and standard deviation among multiple sites in IM (TP). More details about the default value and physical range of each parameter could be found at http://forge.ipsl.jussieu.fr/orchidee/wiki/Documentation/UserGuide.

Parameters	Description	Prior	Post IM (mean ± std.)	Post TP (mean ± std.)
Photosynthesis				
V_{cmax25}	Maximum carboxylation rate at 25 °C (μmol m^{-2} s^{-1})	70 (38–102)	60.6 ± 20.3	66.9 ± 11.9 **
$ARJV$	intercept of linear function of T defining the J_{max25}/V_{cmax25} ratio	2.59 (2–3)	2.6 ± 0.2	2.5 ± 0.1 **
$BRJV$	slope of the linear function of T defining the J_{max25}/V_{cmax25} ratio	−0.035 (−0.07–0)	−0.03 ± 0.02	−0.04 ± 0.01 **
D_V_{cmax}	Energy of deactivation of V_{cmax}	200000 (180000–220000)	202433.5 ± 7585.4	201728.8 ± 6389.7 **
E_V_{cmax}	Energy of activation of V_{cmax}	71513 (57210–85815)	74723.8 ± 5989.7	73964.8 ± 5682.0 **
E_J_{max}	Energy of activation of J_{max}	49884 (39907–59860)	50617.6 ± 4169.0	50595.2 ± 2152.9 **
Phenology				
SLA	Specific leaf area (LAI per dry matter content, m^2 g^{-1})	0.03 (0.013–0.05)	0.03 ± 0.01	0.02 ± 0.01 **
LAI_{max}	Maximum leaf area index (LAI)	2.5 (1.5–3.5)	2.5 ± 0.6	2.5 ± 0.2 **
$K_{LAI,happy}$	LAI threshold to stop carbohydrate use	0.5 (0.35–0.7)	0.5 ± 0.06	0.5 ± 0.04 **
$L_{agecrit}$	Average critical age of leaves (days)	120 (60–180)	122.2 ± 35.3	110.6 ± 19.5 **
$Senescence\_temp\_c$	Constant c for calculating the critical temperature for senescence	−1.4 (−11.375–9.375)	−1.5 ± 0.4	1.6 ± 3.2 **
Soil water availability				
Hum_{cste}	Shape of the root profile (m^{-1})	4 (1–10)	3.6 ± 1.2	3.3 ± 2.0 **
Autotrophic respiration				
MR_b	Offset of the affine relationship between temperature and maintenance respiration	−0.0013 (−0.002 to −0.001)	−0.0015 ± 0.0003	−0.0014 ± 0.0001 **
MR_c	Slope of the affine relationship between temperature and maintenance respiration	0.16 (0.08–0.24)	0.13 ± 0.02	0.16 ± 0.02 **
GR_{frac}	Fraction of biomass available for growth respiration	0.28 (0.2–0.36)	0.29 ± 0.04	0.29 ± 0.02 **
Heterotrophic respiration				
K_{soilC}	Multiplicative factor of initial carbon pools	1 (0.5–2)	0.4 ± 0.4	0.6 ± 0.5 **

** The difference between parameter values of IM and TP sites are significant ($p < 0.01$).

Table 2
The general information of the eddy-covariance (EC) flux sites used in this study on Inner Mongolia (IM) and Tibetan Plateau (TP). ELE is elevation, MAT and MAP are mean annual temperature and precipitation, respectively.

ID	Region	Name	Location	ELE (m)	MAT (°C)	MAP (mm)	Year	Reference
Du2	IM	Duolun	42.05°N,116.28°E	1350	3.05	284.53	2006	Chen et al. (2009)
Xfs	IM	Xilinhot	43.13°N,116.33°E	1030	1.80	84.06	2005	Wang et al. (2008a,b)
Xi1	IM	Xilinhot	43.55°N,116.68°E	1250	2.21	134.37	2006	Chen et al. (2009)
Xi2	IM	Xilinhot	43.55°N,116.67°E	1250	2.05	134.65	2006	Chen et al. (2009)
NaM	IM	Naiman	42.93°N,120.70°E	367	7.81	210.39	2009	Li and Ma (2015)
TNY	IM	Tongyu	44.57°N,122.93°E	151	6.86	268.51	2009	Li and Ma (2015)
HaM	TP	Haibei	37.60°N,101.30°E	3250	−0.73	416.94	2002	Kato et al. (2004)
DXG	TP	Dangxiong	30.50°N, 91.06°E	4333	2.81	315.03	2007	Xu et al. (2005)
ARG	TP	Arou	38.04°N,100.46°E	3033	−0.20	298.50	2010	Wang et al. (2010)

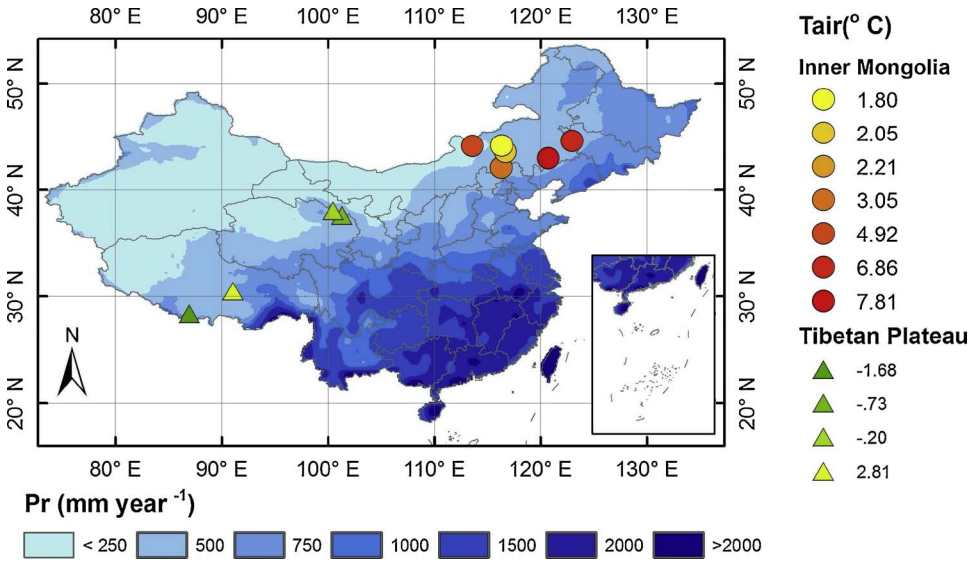

Fig. 1. The location and distribution of eddy-covariance (EC) flux sites used in this study. The base map is the average annual precipitation for the period 1979–2012 (He, 2010). The annual temperature for each site is derived from EC flux measurements. The triangle markers represent sites on Tibetan Plateau, and circle markers illustrate sites on Inner Mongolia.

redundancy, we thus integrated the flux data from half-hourly time step to daily time step for model-data assimilation.

Climate forcing, vegetation and soil texture information are necessary for model simulations. For each EC site, the vegetation type is assigned to C_3 grassland – one of plant functional types (PFTs) in ORCHIDEE. The soil texture parameters used to calculate soil hydrological parameters in ORCHIDEE are derived from the high spatial-resolution soil map of China (Shangguan et al., 2014). The ORCHIDEE model is driven by half-hourly meteorological datasets (Wang et al., 2012). Forcing variables include air temperature, rainfall and snowfall rates, specific humidity, wind speed, pressure, and shortwave and longwave incoming radiations. As some variables were missing in the EC-measured dataset and gaps exist in the EC-measured meteorological records, we reconstructed site-level meteorological forcing by merging the EC site measurements with a gridded meteorological dataset with temporal resolution of 3 h and a spatial resolution of 0.1° × 0.1° over China (He, 2010). This meteorology dataset was produced by merging the 740 station meteorological observations with the Princeton reanalysis dataset (Chen et al., 2011). To merge the EC site measurements with the gridded meteorological dataset, we first averaged the half-hourly site observed records to 3-h time step to match the temporal resolution of the gridded dataset. Then, we corrected the series of corresponding pixels from the gridded dataset against the available EC records through a linear regression equation. Finally, we applied the linear regression equation to correct the gridded dataset and fill the gaps in the EC observed records with the corrected series in the gridded dataset.

2.4. Simulation protocol

We applied ORCHIDEE in a "grid-point" mode, forced by gap-filled meteorological data made on the top of the flux tower. Biomass and soil carbon pools are initialized to steady-state equilibrium from a spin-up run of ORCHIDEE, i.e., a 10,000 year run using average climate forcing data at each site. To investigate the site-level responses of TP and IM grasslands to climate change, we designed a series of idealized simulation experiments with temperature and precipitation annual anomalies applied to current climate conditions. Specifically, temperature anomalies are T + 0.5 °C, T + 1 °C, T + 1.5 °C, T + 2 °C, where T defines current temperature conditions (control simulation). Precipitation relative anomalies are P − 30%, P − 20%, P − 10%, P + 10%, P + 20%, P + 30% around current precipitation.

2.5. Decomposition of annual GPP

In this study, we used the same method to decompose annual GPP under simulations with altered temperature and precipitation following Xia et al. (2015). The GPP_{max} was defined as the maximal daily GPP during the growing season, and CUP was defined as the period between the starting day and ending day of CO_2 uptake period during a year. We first fitted the annual GPP with an idealized curve defining by the Weibull function:

$$P(t) = c\left(\frac{t}{a}\right)^{(b-1)} e^{-\left(\frac{t}{a}\right)^b} \quad (1)$$

where t represents the number of days in each year, and $P(t)$ is the

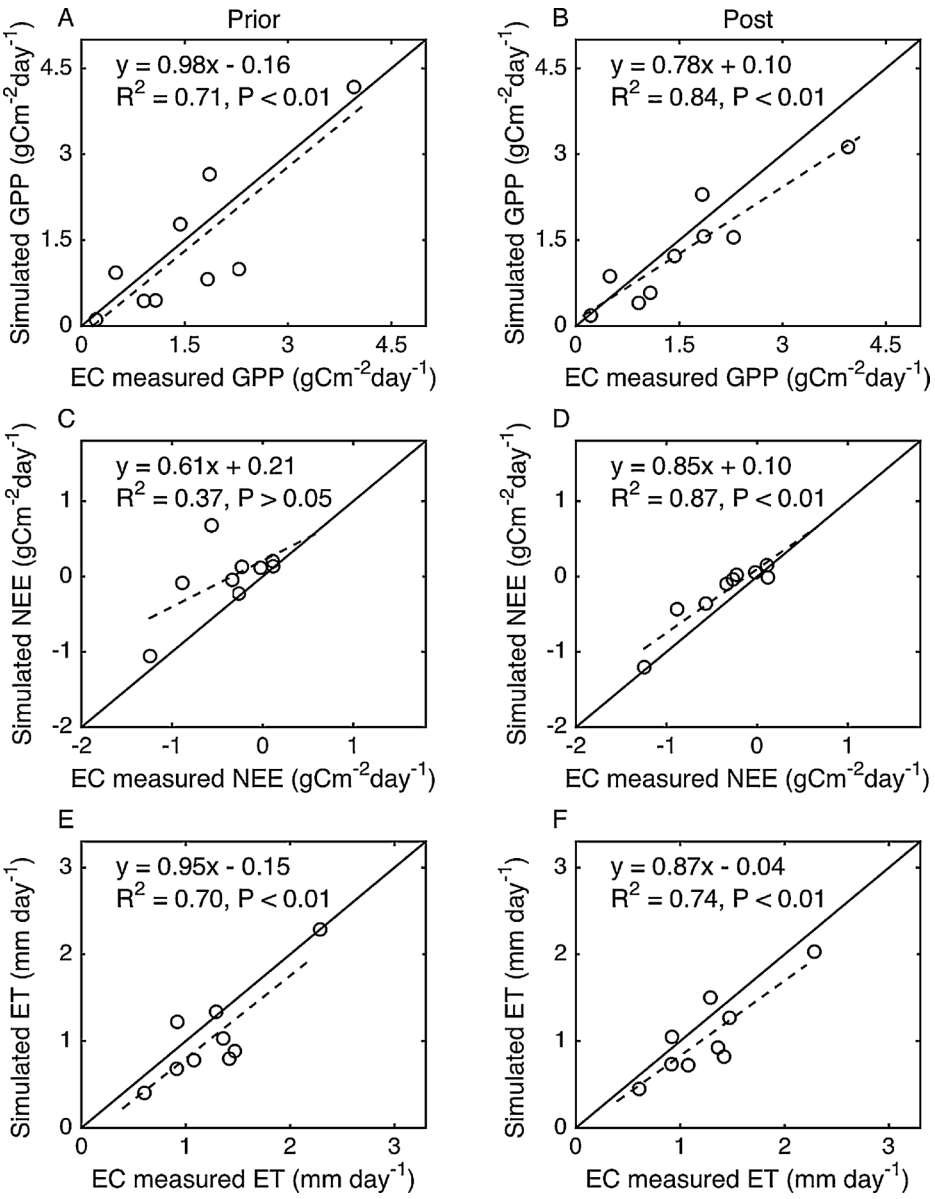

Fig. 2. Comparison between model simulated annual GPP (A, B), NEE (C, D), and ET (E, F) and EC measurements before (prior, left panel) and after (post, right panel) parameter optimization. The dots are annual GPP of each site year.

corresponding daily mean GPP ($gCm^{-2}day^{-1}$), a, b and c are empirical parameters to be estimated. The GPP_{max} was then calculated as:

$$GPP_{max} = max\{P(t)\} \quad (2)$$

The CUP was calculated as

$$CUP = CUP_{end} - CUP_{start} \quad (3)$$

where CUP_{start} (or CUP_{end}) was calculated as the intersection between the recovery line (or senescence line) and the time axis. For more detail about the decomposing method, please see Xia et al. (2015).

3. Results

3.1. Performance of optimized model

The model performance is improved after parameter optimization. The original model (before parameter optimization) well captures cross-site variability in annual GPP from EC measurements (Fig. 2A). The modeled annual GPP explains 71% of cross-site variations of annual GPP and no systematic bias are found (slope = 0.98, Fig. 2A). However, the good performance is not similarly found in the maximum GPP and carbon uptake period (CUP) (Fig. 3A, C) that are decomposed from annual GPP (see Section 2.4). The model captures only 46% of cross-site GPP_{max} variability (Fig. 3A), and 53% of the cross-site CUP variability (Fig. 3C). After the parameter optimization, the correlation coefficient (R^2) of modeled annual GPP to EC-based GPP reaches 0.84 (Fig. 2B), and the model performance on GPP_{max} and CUP is largely improved (Fig. 3B, D). Specifically, the R^2 of modeled GPP_{max} to EC-based GPP_{max} increases from 0.46 to 0.74 and the R^2 of modeled CUP to EC-based CUP increases from 0.53 to 0.75. The parameter optimization also reduces the overall GPP RMSE from 1.27 ± 0.54 $gC\,m^{-2}\,day^{-1}$ in the prior simulations to 1.0 ± 0.48 $gC\,m^{-2}\,day^{-1}$ in the post simulations (Fig. 4). For the prior simulations, the modeled annual average NEE is near zero at most of the sites (Fig. 2C), which can be attributed to the near equilibrium state following spin-up. The model performance on NEE is largely improved in the post simulations, and R^2 increase from 0.37 to 0.87 (Fig. 2C, D) and RMSE reduced from 1.03 ± 0.41 to 0.82 ± 0.36 $gC\,m^{-2}\,day^{-1}$ (Fig. 4). The improvement of model performance on NEE is achieved by reducing the parameters associated with autotrophic respiration and heterotrophic respiration through the optimization process. For instance, the reduction in $K_{soil}C$, which scales the sizes of the initial carbon pools in the post parameter set (from the

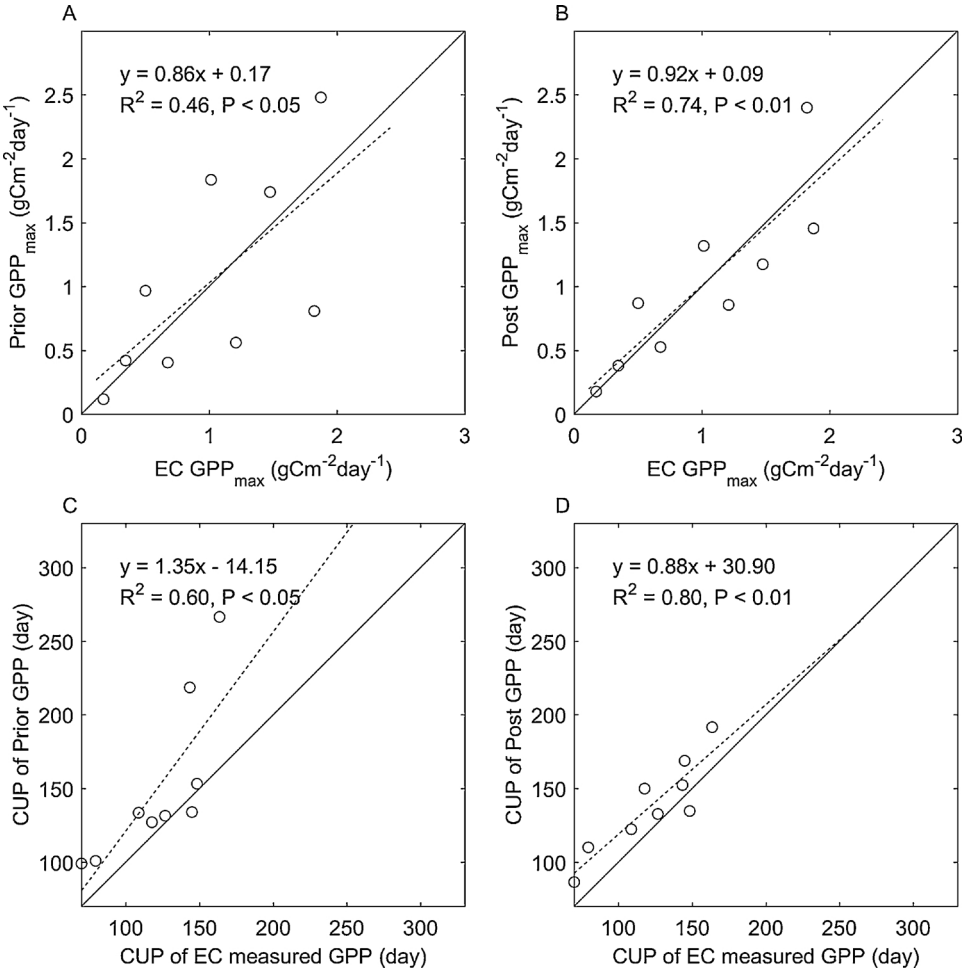
A
y = 0.86x + 0.17
R2 = 0.46, P < 0.05
Prior GPPmax (gCm-2day-1)
EC GPPmax (gCm-2day-1)
B
y = 0.92x + 0.09
R2 = 0.74, P < 0.01
Post GPPmax (gCm-2day-1)
EC GPPmax (gCm-2day-1)
C
y = 1.35x - 14.15
R2 = 0.60, P < 0.05
CUP of Prior GPP (day)
CUP of EC measured GPP (day)
D
y = 0.88x + 30.90
R2 = 0.80, P < 0.01
CUP of Post GPP (day)
CUP of EC measured GPP (day)

Fig. 3. Comparison between GPP_{max} (A, B) and CUP (C, D) derived from modeled GPP and EC estimated GPP. The left panel are results before parameter optimization, and right panel are results after parameter optimization.

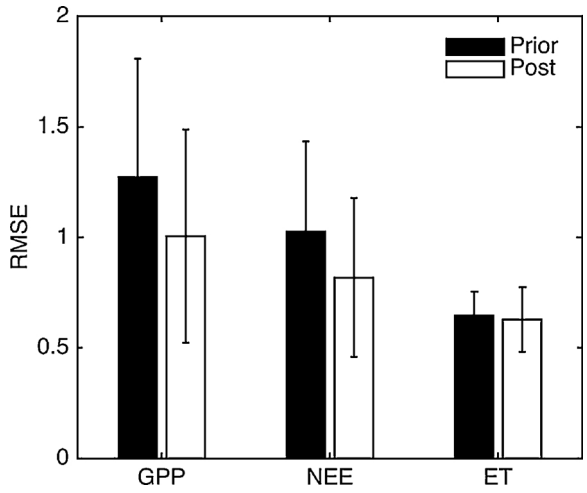

Fig. 4. The model RMSE before (dark bar) and after (white bar) parameter optimization. The bar represents the average RMSE across the EC sites, and the error bar is the standard deviation.

default value of 1.0 to the optimized values of 0.4 ± 0.4 on IM sites, and 0.6 ± 0.5 on TP sites, Fig. S1), decreases the initial soil carbon pool size and thereby reduce the magnitude of R_h, resulting in net carbon sink on most of the sites.

In contrast, the improvement of the model performance on evapotranspiration (ET) is small (Fig. 2E, F). In the prior simulation, the model already well captured the variations of annual ET across sites (R^2 = 0.7, RMSE = 0.65 ± 0.11 mm day^{-1}). The model after parameter optimization have roughly similar performance measured by R^2 and RMSE (R^2 = 0.74, RMSE = 0.63 ± 0.15 mm day^{-1}).

3.2. Responses of carbon fluxes to altered temperature and precipitation

The GPP of grasslands on TP and IM shows opposite responses to warming in the idealized simulations. At the TP sites, the multi-site average annual GPP increases along the warming gradient. In sharp contrast, this result is reversely found on IM sites. For example, when temperature increases by 2 °C, the magnitude of GPP increases by 45.5 ± 67.9 gC m^{-2} $year^{-1}$ on TP sites but decreases by 31.1 ± 31.8 g C m^{-2} $year^{-1}$ on IM sites (Fig. 5A). The multi-site average annual GPP increases with temperature at a rate of 22.43 ± 36.41 g C m^{-2} $year^{-1}$ $°C^{-1}$ on TP, but decreases at a rate of 15.53 ± 15.91 g C m^{-2} $year^{-1}$ $°C^{-1}$ on IM (Fig. 5I). In contrary to temperature, the responses of GPP to altered precipitation regimes are broadly similar on both TP and IM grasslands. In general, GPP increases along wetting condition and decrease under drying condition, but the precipitation sensitivity measured by the slope of annual GPP to annual precipitation along the precipitation gradient differs between TP and IM. The grasslands on TP have an asymmetrical response to drying condition compared to wetting condition. When annual precipitation decreased by 30%, the GPP decreases by 115.4 ± 67.8 g C m^{-2} $year^{-1}$. Under the 30% increase of precipitation, the GPP increases by 49.62 ± 39.31 g C m^{-2} $year^{-1}$ (Fig. 5B). Overall, the GPP increase at a rate of 27.4 ± 18.4 g C m^{-2} $year^{-1}$ per 10% precipitation change. For grasslands on IM, the GPP responds almost linearly to altered precipitation (reduction of 107.1 ± 101.3 g C m^{-2} $year^{-1}$ with 30% reduction of precipitation

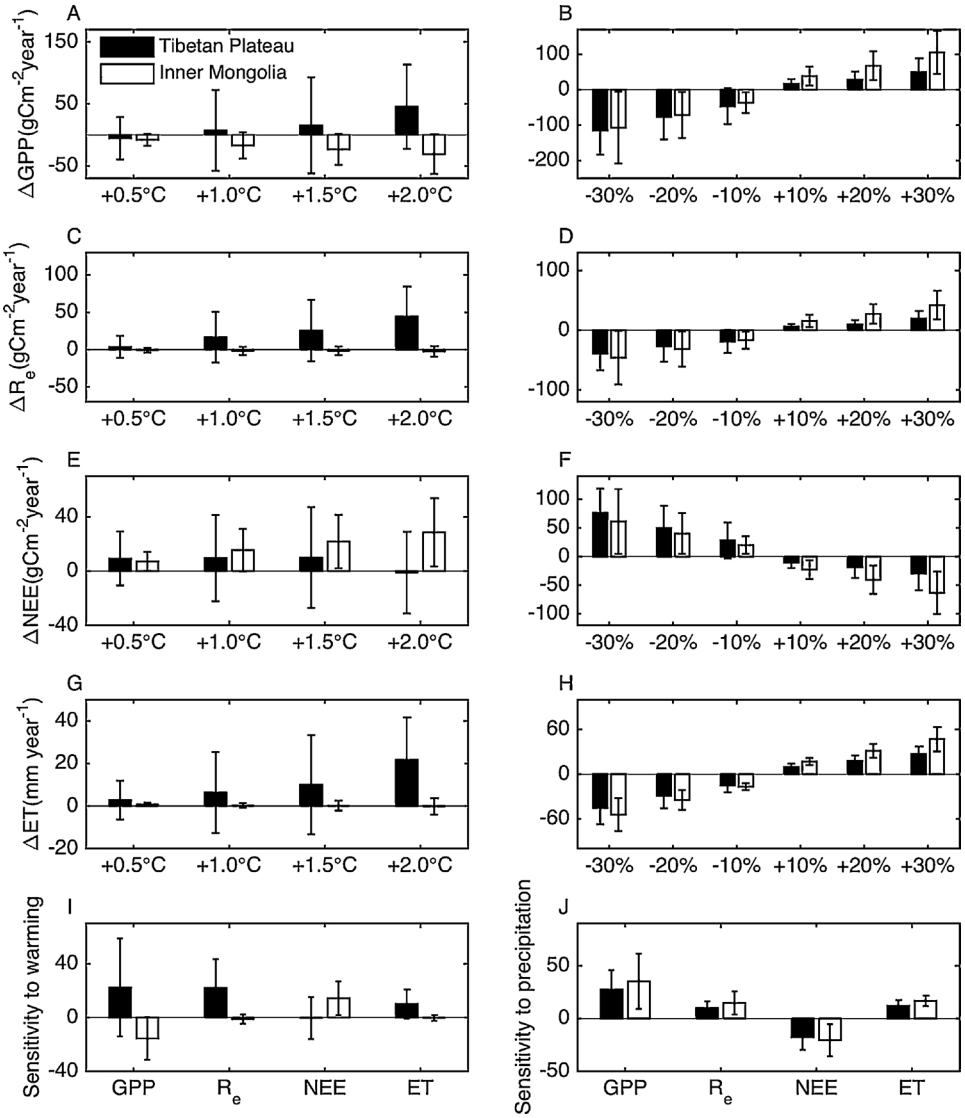

Fig. 5. The response of GPP (A, B), R_e (C, D), NEE (E, F) and ET (G, H) to changing air temperature (left panel) and precipitation (right panel), and their sensitivity to warming (I) and altered precipitation (J). For A-H, the bar represents the average differences of annual fluxes between the warming/altered precipitation experiments and control experiment across the multiple EC sites, and the error bar is multi-site standard deviation. For I and J, the bar is the average sensitivity to warming/altered precipitation among multiple sites, and the error bar is multi-site standard deviation. The dark bar is results from TP sites and white bar is IM sites. The unit of sensitivity to warming is $gCm^{-2}year^{-1}\,°C^{-1}$ for GPP, R_e and NEE, and mm $year^{-1}\,°C^{-1}$ for ET. The unit of sensitivity to altered precipitation is g $Cm^{-2}year^{-1}10\%Pr^{-1}$ and mm $year^{-1}10\%Pr^{-1}$.

and increase of 105.4 ± 60.8 g C m^{-2} $year^{-1}$ with 30% increase of precipitation), increasing at a rate of 35.4 ± 26.1 g C m^{-2} $year^{-1}$ per 10% increase of precipitation, higher than that on TP (Fig. 5).

Evidence is mounting that the production of GPP_{max} and CUP could explain most of temporal and spatial annual GPP variations (Xia et al., 2015). In this study we also decomposed annual GPP to GPP_{max} and CUP to investigate the relative importance of GPP_{max} and CUP in regulating the responses of GPP to warming and altered precipitation. In the warming simulations, the variance of GPP_{max} nearly explains ~80% and ~100% of the variance of annual GPP anomaly across IM and TP sites, respectively. Similar results are also found in the altered precipitation simulations. In the warming simulations, we find the negative relationship between annual GPP and CUP across IM sites, indicating longer CUP but less GPP in the warming condition. No significant relationship is found between annual GPP and CUP on TP sites. In the altered precipitation simulations, the relationship between annual GPP and CUP is weak on both TP and IM sites (Fig. 6).

Similar to GPP, the changes in R_e shows contrasting responses to warming between TP and IM sites. For the TP sites, the site average R_e increases at a rate of 22.1 ± 21.4 g C m^{-2} $year^{-1}$ $°C^{-1}$ along the warming gradient, with the increment reaching 44.4 ± 39.9 g C m^{-2} $year^{-1}$ when temperature increases by 2 °C (Fig. 5C). As R_e and GPP increase at the comparable rates with warming, the change in NEE is rather small (Fig. 5E). At the Inner Mongolian sites, the R_e decrease slightly with temperature at a rate of 1.17 ± 3.56 g C m^{-2} $year^{-1}$ $°C^{-1}$. The reduction of GPP is larger than that of R_e, therefore shifting NEE to less carbon uptake. The R_e responses to altered precipitation regime are similar on both TP and IM grasslands. For the TP sites, a 30% increase of precipitation leads to an increase of 19.72 ± 12.53 g C m^{-2} $year^{-1}$ in R_e, which is smaller than that of GPP, leading to decreasing NEE (stronger CO_2 sink) across TP sites. For the IM sites, the same increase of precipitation leads to 42.02 ± 24.12 g C m^{-2} $year^{-1}$ increase in R_e. The smaller increase of C loss from R_e than C uptake from GPP results in stronger CO_2 sink or weaker CO_2 source across the six sites on IM.

The changes in carbon fluxes show different patterns in TP and IM under simulations considering an interaction of different warming rates and varying precipitation levels. For the TP grasslands, the warming-induced increases in GPP and Re are amplified as precipitation increases (Fig. 11A, C). Given that warming-induced increase in GPP and Re increases at a comparable rate along an increasing precipitation gradient, the warming-induced changes in NEE thus varies little (Fig. 11 E). Under the drying condition, warming also stimulates GPP and Re even if precipitation decreases by 30%. However, under the severe drying condition (precipitation decreases by 30%), the warming-induced increases Re is larger than that of GPP, and then results in more carbon loss in response to warming. In the IM grasslands, however, the changes of Re in response to warming and altered precipitation are

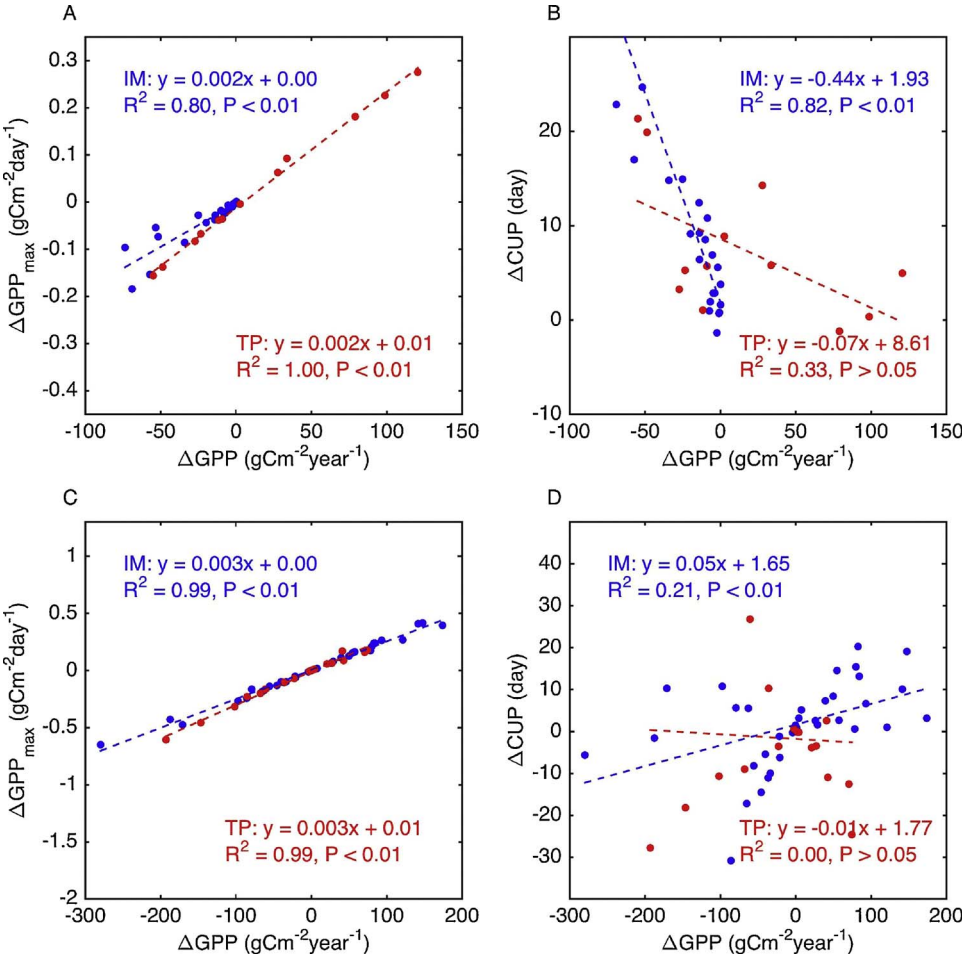

Fig. 6. The dependence of annual GPP anomaly on GPP_{max} anomaly (left panel) and CUP anomaly (right panel). The anomalies are calculated as the difference between warming/altered precipitation simulations with control simulations. The upper panel (A and B) are results from warming simulations and bottom panel (C and D) are from altered precipitation simulations. Blue dots are IM sites, and red dots are TP sites. Each dot represents simulation at each altered temperature or precipitation gradient at each site. (For interpretation of the references to colour in this figure legend, the reader is referred to the web version of this article.)

much smaller than those of GPP. The suppressed GPP under warming exists under both decreasing and increasing precipitation conditions. As a result, the NEE decreases (more carbon gain) under a combination of the current temperature and increasing precipitation condition, while it increases (more carbon release) under the drier and warmer climate (Fig. 11F).

3.3. Responses of water fluxes to altered temperature and precipitation

At the TP sites, the ET increases at a rate of 12.02 ± 5.38 mm $year^{-1}$ $°C^{-1}$ (Fig. 5I). This increase in ET is mainly attributed to the increase in transpiration, indicating enhanced vegetation activities under warming condition on TP (Fig. 7). Enlarged LAI under warming, which increase from 0.7 ± 0.3 in the control simulation to 0.8 ± 0.4 in the T + 2 °C simulation, is the major factor responsible for the increase of transpiration (Fig. 8A). We also calculated the ratio of transpiration to LAI (T/LAI) as a proxy of stomata conductance at the ecosystem level. The results show that the T/LAI is almost consistent in the warming simulations, indicating negligible changes of stomata conductance under warming on TP sites (Fig. 8C). Moreover, our simulations show that transpiration accounts for about 56 ± 7% of ET across sites, and this ratio remains constant along the warming gradient (Fig. 9A). On the IM sites, however, the changes on ET are negligible (Fig. 5G). By analyzing the three components of ET, we find decreasing transpiration under warming, indicating that the vegetation activities are suppressed under warming condition on IM sites. The decrease of transpiration is compensated by the increase of soil evaporation, resulting in negligible change in ET (Fig. 7B). The decreasing transpiration on IM also results from changes in LAI (decreased from 0.40 ± 0.3 in the control simulation to 0.37 ± 0.24 in the T + 2 °C simulation). The T/LAI is stable at around 1.15 mm day^{-1} in the warming simulations (Fig. 8). On the IM sites, the percentage of transpiration to ET is lower than TP (49 ± 14% at the control simulation), and the T/ET ratio decreases at a rate of 1 % $°C^{-1}$ along the warming gradient (Fig. 9).

The ET responses to wetting or drying are similar on TP and IM. The cross-site ET increases by 47 ± 16.3 and 27.17 ± 10 (mm $year^{-1}$ per 30% increase in precipitation) on IM and TP, and decreases by 54.4 ± 22.1 and 45.5 ± 21. 8 (mm $year^{-1}$ per 30% decrease in precipitation) on IM and TP, respectively. As shown in Fig. 7, the changes of ET with altered precipitation are dominated by transpiration changes under both drying and wetting conditions, highlighting the important role of vegetation activities in the responses of ET to climate change on both TP and IM regions. The changes of transpiration under altered precipitation resulted from changes in LAI, which increased from 0.5 ± 0.3 in the −30% simulation to 0.8 ± 0.2 in the +30% on TP, and from 0.27 ± 0.16 in the −30% simulation to 0.53 ± 0.35 in the +30% simulation on IM. The T/LAI is stable on IM sites under both drying and wetting, and is stable on TP sites under drying while decreases under wetting. With the increasing precipitation, the percentage of transpiration to ET also increases on both TP and IM with large rate on IM than on TP (2% per 10% increase in precipitation on IM and 1% per 10% increase in precipitation on TP).

4. Discussion

4.1. Contrasting responses of carbon fluxes to climate change on TP and IM grasslands

Climate change, especially warming and altered precipitation

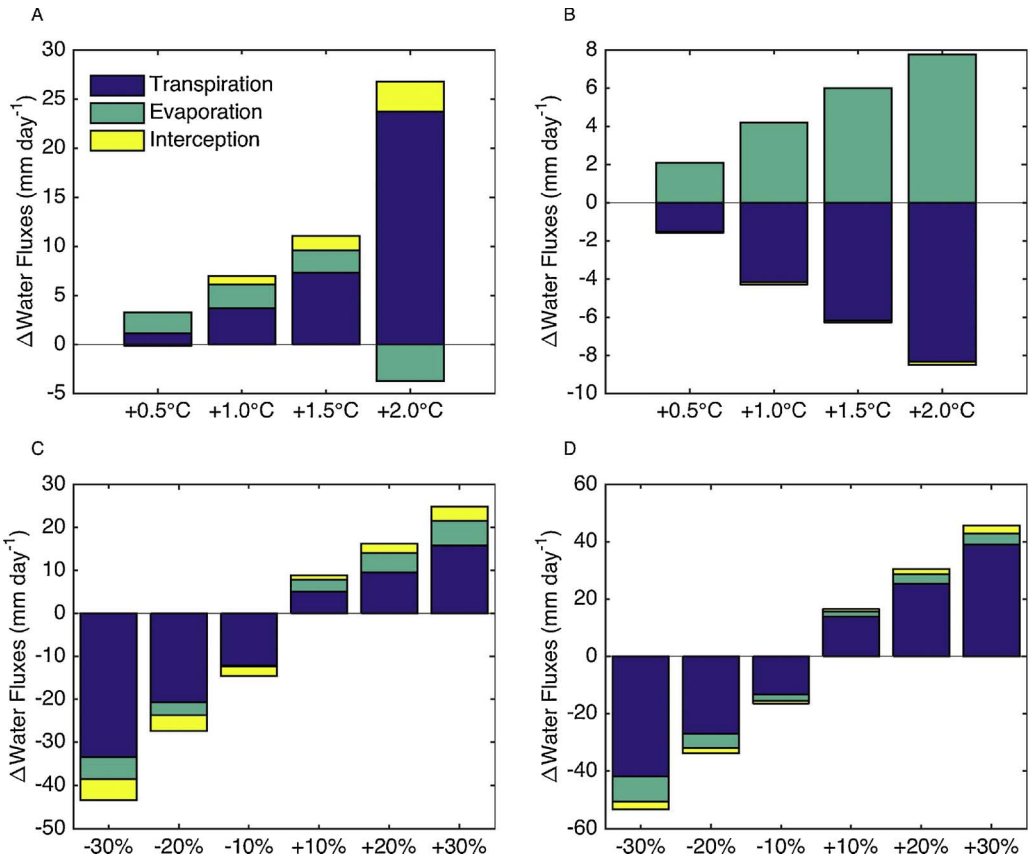

Fig. 7. The changes of transpiration (blue bars), evaporation (green bars) and interception (yellow bars) under warming (A and B) and altered precipitation (C and D) simulations of sites on TP (left panel) and IM (right panel). The values are calculated as multiple site average. (For interpretation of the references to colour in this figure legend, the reader is referred to the web version of this article.)

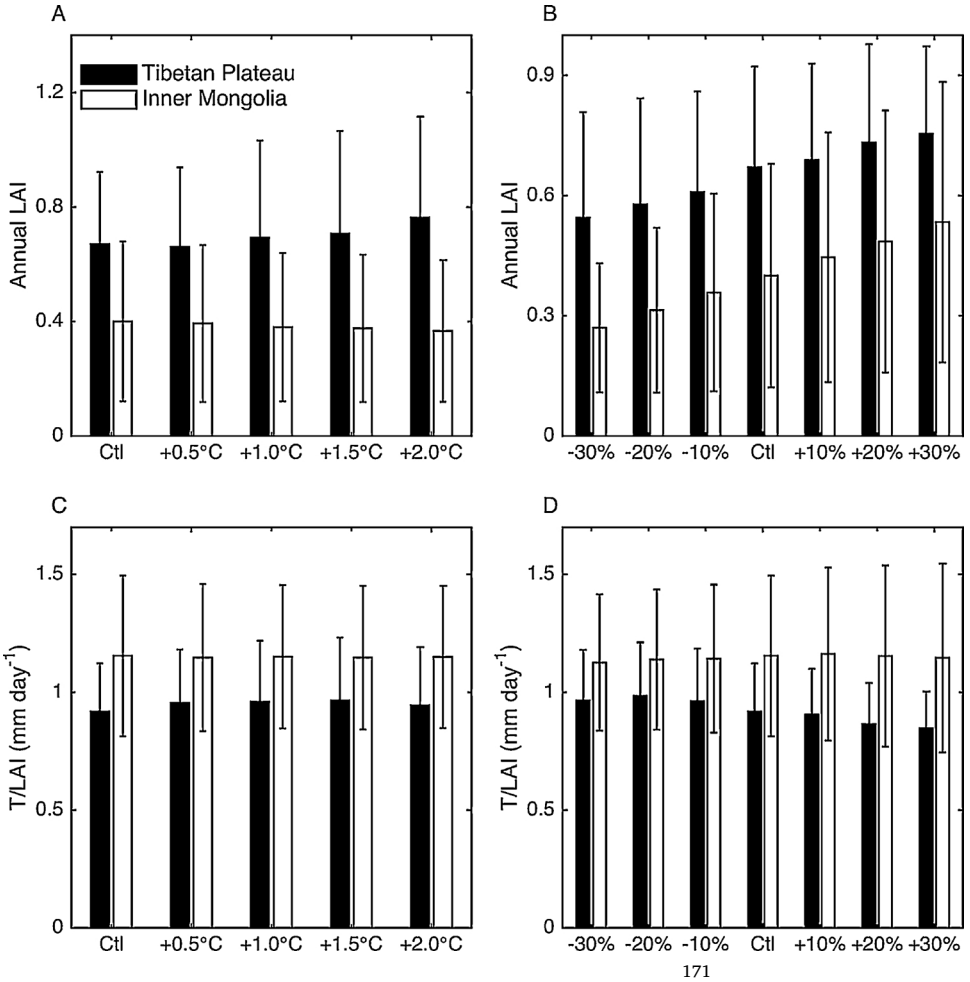

Fig. 8. The changes of annual average LAI (A, B) and ratio of transpiration to LAI (T/LAI, C and D) under warming (left panel) and altered precipitation (right panel) simulations. The black bar is site average for TP sites and white bar is site average for IM sites. The error bar is standard deviation across sites.

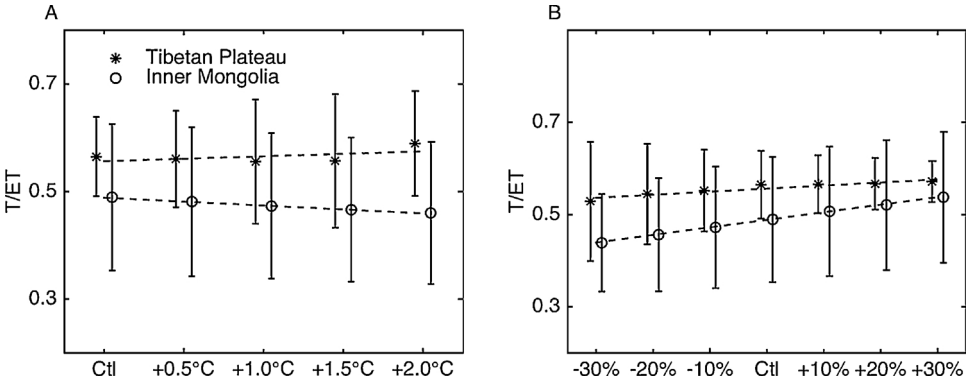

Fig. 9. The ratio of transpiration to ET (T/ET) of warming (A) and altered precipitation simulations (B). The stars are TP results and open dots are IM results. Each dot represents average from multiple sites and error bar is standard deviation. The dash line is the linear regression line of array from warming/altered precipitation gradient.

regime, has profound influence on vegetation activities (Piao et al., 2006; Shen et al., 2011). The increasing temperature has the two-fold effects on vegetation carbon cycle processes. On the one hand, warming enhances the maximum carbon uptake capacity and alters the phenology phase of grassland (Shen et al., 2011; Shen et al., 2013). On the other hand, warming may increase transpiration and enhance the water loss from soil, which in turn result in warm-induced drought that limits photosynthesis and respiration processes (Niu et al., 2008b). This negative effect, however, can be offset or enhanced by altered precipitation regimes and hydrological conditions. These opposing effects of warming could vary among regions characteristic with different climate features.

Alpine grasslands on TP are supposed to be mainly limited by thermal conditions. Increasing temperature is expected to relax the thermal limitation (Du et al., 2004), enhance vegetation activities and stimulate both photosynthesis and respiration processes. Our optimized simulations showed that warming generally results in increase of GPP at TP grasslands, and the increase in GPP is mainly contributed by the increase in maximum photosynthesis capacity. This warming-stimulated increase in productivity is also found based on several manipulative experiments (Pent et al., 2014; Li et al., 2017a). For example, Peng et al. (2014) conducted warming experiment near the Beilu River research station on TP, and found increasing GPP in the warming treatment. The warming experiments conducted by Li et al. (2017a) found significant increase of total biomass after two years of warming on the two meadows in the Fenghuoshan region in the hinterland of TP.

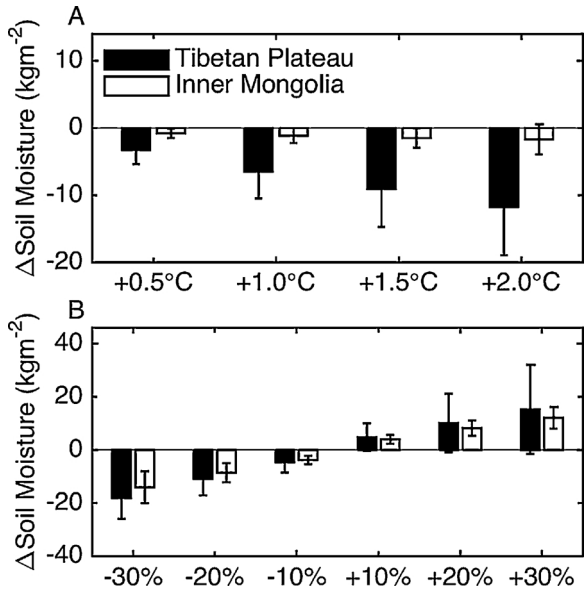

Fig. 10. Changes in soil moisture during the growing season (June to September). The bar represents the average differences of growing season soil moisture between the warming/altered precipitation experiments and control experiment across the multiple EC sites, and the error bar is multi-site standard deviation. The dark bar is results from TP sites and white bar is IM sites.

Warming also alters the CUP, while their effect on GPP varies among sites, indicating large spatial variations of responses to warming on TP. This result is also consistent with the recent satellite-based studies on TP, which shows that the responses of spring phenology and summer greenness to warming are not spatially coherent over the last 3 decades (Shen et al., 2015b; Shen et al., 2016). Several field studies reported reduction of ecosystem production and biomass under warming. For instance, Klein et al. (2007) found aboveground NPP deceased by 10–40 $gCm^{-2}year^{-1}$ in the warming treatment at the Haibei alpine research station. Fu et al. (2013) reported decreased GPP and above ground biomass by 21.7% to 23.0% and 17.1% on a south-facing slope on the Nyainqentanglha Mountains following 0.94 °C to 1.81 °C of warming. Moreover, warming increases R_e on TP sites (Fig. 5C). As GPP and R_e increase at comparable rate with temperature, the NEE change is negligible. Piao et al. (2012) analyzed the impacts of climate on carbon balance of TP grasslands based on ORCHIDEE model and found similar results that increasing temperature boost NPP, while its effect on NEP is negligible because of the warming-stimulated carbon loss from respiration. Warming is expected to initially stimulate vegetation growth in the alpine ecosystem until the temperature reaches an optimal value, and further warming may suppress vegetation activities.

Our simulations showed decreasing GPP, R_e and weakening carbon uptake in the drying condition and increasing production and respiration in the wetting condition (Fig. 5). Zhang et al. (2013) found strong positive relationship between the annual precipitation amount and the aboveground biomass at the Husbandry Meteorology of Qumalai county observation station on the southeast of TP. The model-based study from Piao et al. (2012) suggests precipitation regime contributes 52% of the increase of NPP on TP and is the primary controlling factor over the central and southwestern TP during 1961–2009. As warming stimulates vegetation growth in this cold ecosystem, it also increases the water demand. Although vegetation growth TP is mainly limited by thermal condition, the shifting precipitation regime is critical for the carbon balance on TP.

In contrast to TP, our simulations suggest decreasing GPP and R_e under warming condition, resulting in weakened carbon sink on IM. On the semi-arid regions, water is the main factor limiting ecosystem production (Huxman et al., 2004; Knapp and Smith, 2001). Increasing temperature could result in decreasing soil water content and the depleted soil water in turn limit the water supply for vegetation growth (Niu et al., 2008b). In our simulations, we found decreasing growing season surface soil moisture with increasing temperature on IM sites, indicating the limitation of water on the vegetation activity in IM (Fig. 10). Moreover, warming induced reduction in soil water could suppress the root and microbial activities, thus leading to decreasing ecosystem respiration. This warming induced increase of NEE (less CO2 uptake) in Inner Mongolia grassland is consistent with previous field

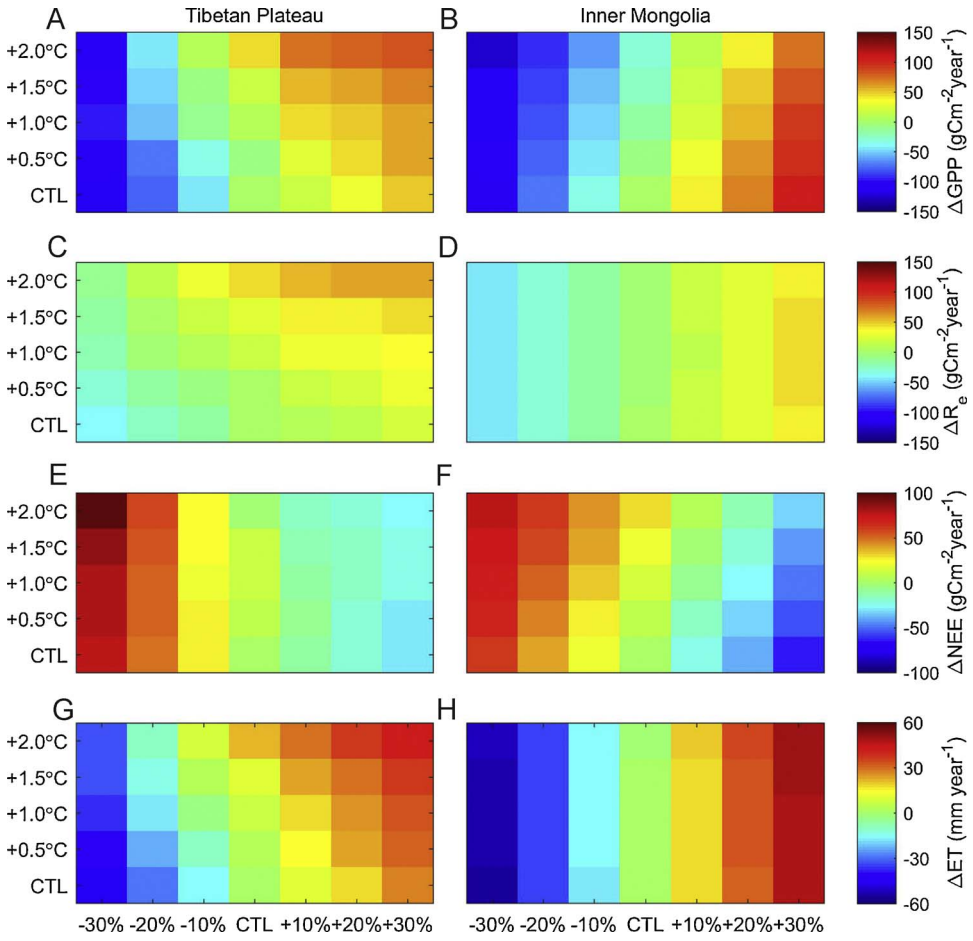

Fig. 11. Changes in GPP (A, B), R_e (C, D), NEE (E, F) and ET (G, H) in altered temperature and precipitation simulations overTibetan Plateau sites (left panel) and Inner Mongolia sites (right panel). The changes of each variable are calculated as average across sites.

experiment studies. For example, *Niu* et al. [2008b] reported that warming on a temperate steppe in Inner Mongolia results in a decrease of GPP and NEP by 11.1% and 12.3%, respectively.

The negative effect of warming on carbon cycle on IM could be alleviated by increasing precipitation. As expected, the increasing precipitation could result in an increase in both GPP and R_e, further leading to decreasing NEE (more carbon uptake) in the wetting condition (Fig. 5). The stimulated of ecosystem carbon fluxes has also been reported in other grassland ecosystems (Hastings et al., 2005; Harper et al., 2005). Higher GPP under increasing precipitation could result from higher photosynthesis rate and altered duration of carbon uptake. Our simulation results suggest that stimulated maximum photosynthesis rate is the major driver of the elevated production under altered precipitation regime (Fig. 6).

Schwalm et al. (2010) investigated the sensitivity of carbon fluxes to evaporative fraction (EF), which is an index of site water status. They found ~50% higher sensitivity of production (GPP) to drought than ecosystem respiration (Re). Our model simulations also showed much higher sensitivity of GPP than that of Re to the water status. For example, in the simulations with altered precipitation, the GPP increases at a rate of 27.4 ± 18.4 and 35.4 ± 26.1 ($g\,C\,m^{-2}\,year^{-1}$ per 10% increase of precipitation) in Tibetan Plateau (TP) and Inner Mongolia (IM) grasslands, respectively. In contrast, the Re increases at a much lower rate of 9.83 ± 6.56 and 14.79 ± 11.01 ($g\,C\,m^{-2}\,year^{-1}$ per 10% increase of precipitation) in TP and IM, respectively.

We should recognize the potential limitations of our model-based global change studies. Previous studies have shown that GPP might acclimate to temperature change through increasing optimum photosynthetic temperature in a warmer environment (Baldocchi et al., 2001; Niu et al., 2012). Furthermore, ecosystem respiration also acclimates to temperature change with decreasing temperature sensitivity at higher temperatures when the moisture supply was not limited [e.g. Luo et al., 2001; Piao et al., 2010]. Our findings based on different rates of the warming treatment might be biased since virtually the majority of state-of-the-art ecosystem carbon cycle models including the optimized ORCHIDEE do not consider the temperature acclimation in their temperature response functions.

4.2. Response of water fluxes to climate change

In this study our simulations showed that transpiration change is the dominant component that driving changes in ET under warming and altered precipitation on both TP and IM grasslands. Under the control, the T/ET ratio was estimated to be 0.56 ± 0.07 and 0.49 ± 0.14 on TP and IM grasslands, respectively. The important role of transpiration on the changes of ET has been reported by many studies. Jasechko et al. (2013) reported that transpiration accounts for 80–90% of global ET based on the isotopic analyses in global lake system. Coenders-Gerrits et al. (2014) reported smaller and larger range of T/ET ratio of 35–80% at global scale. Hu et al. (2008) estimated the partitioning of ET at three TP sites and one IM site based on a two-source model and reported the growing season T/ET to be 0.42–0.59 on TP sites and 0.41 at Neimeng temperate steppe located in Inner Mongolia. Our model estimated T/ET ratio is in a reasonable range and comparable with the previous studies.

As the major component of ET, transpiration links vegetation activities with the regional water cycle and surface energy budget. Its response to climate change could influence the energy fluxes and further affect regional climate. Previous study by Shen et al. (2015a) found that the warming-stimulated increasing vegetation activities on TP could increase the evapotranspiration, resulting in evaporative cooling and providing the negative feedback to regional climate. We found that the transpiration increases with temperature on TP, implying that

human-induced temperature increase in the future might be partially offset by the evaporative cooling effect. In contrast, this effect might not be found on IM grasslands since plant transpiration reduces with increasing temperature. Furthermore, our simulations suggested an increasing T/ET ratio under warming and wetting conditions, indicating an increasing important role of vegetation activities on regulation of surface water and energy fluxes, which could accelerate the negative feedback on climate warming on TP.

5. Conclusions

We are the first to develop a suit of optimized parameter set for the two grasslands from Tibetan Plateau and Inner Mongolia using currently available EC sites. More importantly, we adopt an optimized model-centric approach to identify the differential climate change impacts on atmosphere-biosphere exchanges between the two grasslands. Our results showed that the optimized parameter set is significantly different between TP and IM grasslands, therefore challenging the application of the same parameter set in simulations and/or projection of regional carbon and water budgets in previous modeling studies (Kuppel et al., 2012). The key model parameters that identified here could simplify future model calibrations, and are very valuable to re-evaluate climate change impacts on grassland water and carbon balances at the regional scale. We intend to study this in our follow-up paper. Moreover, the gained knowledge from our modeling results can also be used as guidelines in helping us avoiding manipulative experiments with too many purposes.

However, we should be informed that the evaluation of carbon and water cycles under hypothesized climate change scenario is still not well constrained. On the one hand, the model uncertainty due to parameter misspecification can be eliminated but that due to missing processes (such as adaptation, grassland community dynamics, and carbon–nitrogen interactions) is not resolved. On the other hand, we only considered the effect of altered temperature and precipitation, without including other factors in particular increasing atmosphere CO_2 concentration and human-induced grazing effect. Clearly constraining the related parameters in model using the data from manipulation experiments on grazing and CO_2 fertilization effect is necessary in the future work for a more comprehensive understanding of grasslands response to climate change in these two distinctive regions.

Lastly, one potential criticism could be that our model-based result (i.e. the different processes underlying the responses of water and carbon cycles to warming in IM and TP grasslands) is not verified based on observations. Some groups have provided gridded carbon (GPP and NEE) and water component fluxes (ET) at a global scale (Jung et al., 2010). However, they have been criticized by their poor performance in capturing the inter-annual variation (Piao et al., 2013). These products would then not be suitable for teasing out climate change impacts on water and carbon fluxes using their inter-annual variations. Furthermore, these data-driven products such as GPP have mostly relied upon data (such as EC sites) from forest sites in northern temperate regions, with a very poor coverage of grasslands from Tibetan Plateau and Inner Mongolia. To robustly obtain the observed climate change impact on grassland carbon and water fluxes in TP and IM, it necessitates the development of our own data-driven product that should integrate various data sources such as inventory data (e.g. biomass and soil carbon), flux measurements and satellite observations.

Acknowledgements

We thank Dr. Kun Yang for providing the China meteorological forcing data. The flux data of Du2, Xfs, Xi1, Xi2 sites were derived from the global FLUXNET database (http://www.fluxdata.org/). The flux data of HaM site was derived from AsiaFLUX (http://www.asiaflux.net). The high spatial resolution soil database was downloaded from the Land-Atmosphere Interaction Research Group at Beijing Normal University (http://globalchange.bnu.edu.cn/research/soilw). We appreciate the team from the ORCHIDEE Data Assimilation System (https://orchidas.lsce.ipsl.fr/index.php) for the technique support on the code of the model and the model-data fusion framework. We also thank the reviews for comments and suggestions on this work. This study was supported by Key Research and Development Programs for Global Change and Adaptation (Grant 2017YFA0603604), International Partnership Program of Chinese Academy of Sciences (Grant 131C11KYSB20160061), National Natural Science Foundation of China (Grant 41530528) and the Thousand Youth Talents Plan project in China.

Appendix A. Supplementary data

Supplementary data associated with this article can be found, in the online version, at https://doi.org/10.1016/j.agrformet.2017.11.034.

References

Bacour, C., et al., 2015. Joint assimilation of eddy covariance flux measurements and FAPAR products over temperate forests within a process-oriented biosphere model. J. Geophys. Res.-Biogeosci. 120, 1839–1857.

Baldocchi, D.D., et al., 2001. FLUXNET: A new tool to study the temporal and spatial variability of ecosystem-scale carbon dioxide, water vapor, and energy flux densities. Bull. Am. Meteorol. Soc. 82 (11). http://dx.doi.org/10.1175/1520-0477(2001)082<2415:FANTTS>2.3.CO;2.

Baldocchi, D.D., 2003. Assessing the eddy covariance technique for evaluating carbon dioxide exchange rates of ecosystems: past present and future. Global Change Biol. 9 (4), 479–492.

Ball, J., Woodrow, T., Berry, J., 1987. A model predicting stomatal conductance and its contribution to the control of photosynthesis under different environmental conditions. Prog. Photosynth. 4, 221–224.

Briske, D.D., et al., 2015. Strategies to alleviate poverty and grassland degradtion in Inner Mongolia: intensification vs production efficiency of livestock systems. J. Environ. Manage. 152, 177–182.

Chen, S., Chen, J., Lin, G., Zhang, W., Miao, H., Wei, L., Huang, J., Han, X., 2009. Energy balance and partition in Inner Mongolia steppe ecosystems with different land use types. Agric. Forest Meteorol. 149 (11), 1800–1809. http://dx.doi.org/10.1016/j.agrformet.2009.06.009.

Chen, Y., Yang, K., He, J., Qin, J., Shi, J., Du, J., He, Q., 2011. Improving land surface temperature modeling for dry land of China. J. Geophys. Res. Atmos. 116 (116), 999–1010.

Chi, Y.G., et al., 2013. Acclimation of foliar respiration and photosynthesis in response to experimental warming in a temperate steppe in Northern China. PLoS One 8 (2), e56482. http://dx.doi.org/10.1371/journal.pone.0056482.

Coenders-Gerrits, A.M.J., van der Ent, R.J., Bogaard, T.A., Wang-Eriandsson, L., Hrachowitz, M., Savenije, H.H.G., 2014. Uncertainties in transpiration estimates. Nature 506 (7487), E1–E2.

Collatz, G., Ribas-Carbo, M., Berry, J., 1992. Coupled photosynthesis-stomatal conductance model for leaves of C_4 plants. Aust. J. Plant Physiol. 19, 519–538.

Du, M.Y., Kawashima, S., Yonemura, S., Zhang, X., Chen, S., 2004. Mutual influence between human activities and climate change in the Tibetan Plateau during recent year. Global Planet. Change 41 (3–4), 241–249.

Farquhar, G., von Gaemmener, S., Berry, J., 1980. A biochemical model of photosynthesis CO_2 fixation in leaves of C_3 species. Planta 149, 78–90.

Fu, G., Zhang, X., Zhang, Y., Shi, P., Li, Y., Zhou, Y., Yang, P., Shen, Z., 2013. Experimental warming does not enhance gross primary production and above-ground biomass in the alpine meadow of Tibet. J. Appl. Remote Sens. 7 (1). http://dx.doi.org/10.1117/1.JRS.7.073505. (073505-073505).

Gong, D.Y., Shi, P.J., Wang, J.A., 2004. Daily precipitation changes in the semi-arid region over northern China. J. Arid Environ. 59 (4), 771–784.

Harper, C.W., Blair, J.M., Fay, P.A., Knapp, K., Carlisle, J.D., 2005. Increased rainfall variability and reduced rainfall amount decreases soil CO_2 flux in a grassland ecosystem. Global Change Biol. 11, 322–344.

Hastings, S.J., Oechel, W.C., Muhlia-Melo, A., 2005. Diurnal, seasonal and annual variation in the net ecosystem CO_2 exchange of a desert shrub community (Sarcocaulescent) in Baja California, Mexico. Global Change Biol. 11, 927–939.

He, J., 2010. Development of Surface Meteorological Dataset of China with High Temporal and Spatial Resolution, Beijing.

Hu, Z., Yu, G., Fu, Y., Sun, X., Li, Y., Shi, P., Wang, Y., Zheng, Z., 2008. Effects of vegetation control on ecosystem water use efficiency within and among four grassland ecosystems in China. Global Change Biol. 14, 1609–1619.

Huxman, T.E., et al., 2004. Convergence across biomes to a common rain-use efficiency. Nature 429 (6992), 651–654. http://www.nature.com/nature/journal/v429/n6992/suppinfo/nature02561_S1.html.

IPCC, 2013. Climate change 2013: the physical science basis. In: Contribution of Working Group I to the Fifth Assessment Report of the Intergovernmental Panel on Climate Change. Cambridge University Press, Cambridge, United Kingdom and New York, NY, USA. pp. 1535. http://dx.doi.org/10.1017/CBO9781107415324.

Ishida, A., Uemura, A., Koike, N., Matsumoto, Y., Lai Hoe, A., 1999. Interactive effects of

leaf age and self-shading on leaf structure, photosynthetic capacity and chloropyII fluorescence in the rain forest tree, dryobalanops aromatica. Tree Physiol. 19, 741–747.
Jasechko, S., Sharp, Z.D., Gibson, J.J., Birks, S.J., Yi, Y., Fawcett, P.J., 2013. Terrestrial water fluxes dominated by transpiration. Nature 496, 347–351.
Jung, M., et al., 2010. Recent decline in the global land evapotranspiration trend due to limited moisture supply. Nature 467, 951–954. http://dx.doi.org/10.1038/nature09396.
Kang, L., Han, X., Zhang, Z., Sun, O.J., 2007. Grassland ecosystems in China: review of current knowledge and research advancement. Phil. Trans. R. Soc. B : Biol. Sci. 362 (1482), 997.
Kato, T., Tang, Y., Gu, S., Cui, X., Hirota, M., Du, M., Li, Y., Zhao, X., Oikawa, T., 2004. Carbon dioxide exchange between the atmosphere and an alpine meadow ecosystem on the Qinghai–Tibetan Plateau, China. Agric. Forest Meteorol. 124 (1–2), 121–134. http://dx.doi.org/10.1016/j.agrformet.2003.12.008.
Kato, T., Tang, Y., Song, G.U., Hirota, M., Mingyuan, D.U., Yingnian, L.I., Zhao, X., 2006. Temperature and biomass influences on interannual changes in CO2 exchange in an alpine meadow on the Qinghai-Tibetan Plateau. Global Change Biol. 12 (7), 1285–1298.
Klein, J.A., Harte, J., Zhao, X.Q., 2007. Experimental warming not grazing, decreases rangeland quality on the Tibetan Plateau. Ecol. Appl. 17 (2), 541–557.
Knapp, A.K., Smith, M.D., 2001. Variation among biomes in temporal dynamics of aboveground primary production. Science 291 (5503), 481.
Krinner, G., Viovy, N., Noblet-Ducoudré, N.D., Ogée, J., Polcher, J., Friedlingstein, P., Ciais, P., Sitch, S., Prentice, I.C., 2005. A dynamic global vegetation model for studies of the coupled atmosphere-biosphere system. Global Biogeochem. Cycles 19 (1) 56–56.
Kuppel, S., Peylin, P., Chevallier, F., Bacour, C., Maignan, F., Richardson, A.D., 2012. Constraining a global ecosystem model with multi-site eddy-covariance data. Biogeosciences 9 (10), 3757–3776. http://dx.doi.org/10.5194/bg-9-3757-2012.
Kuppel, S., Chevallier, F., Peylin, P., 2013. Quantifying the model structural error in carbon cycle data assimilation system. Geosci. Model Dev. 6, 45–55. http://dx.doi.org/10.5194/gmd-6-45-2013.
Kuppel, S., Peylin, P., Maignan, F., Chevallier, F., Kiely, G., Montagnani, L., Cescatti, A., 2014. Model-data fusion across ecosystems: from multisite optimizations to global simulations. Geosci. Model Dev. 7 (6), 2581–2597.
Lasslop, G., et al., 2008. Influences of observation errors in eddy flux data on inverse model parameter estimation. Biogeosciences 5, 1311–1324.
Li, M., Ma, Z., 2015. Sensible and latent heat flux variability and response to dry–wet soil moisture zones across China. Boundary Layer Meteorol. 154 (1), 157–170. http://dx.doi.org/10.1007/s10546-014-9963-x.
Li, G.Y., et al., 2017a. Effects of warming and increased precipitation on net ecosystem productivity: a long-term manipulative experiment in a semiarid grassland. Agric. Forest Meteorol. 232, 359–366.
Li, Y., et al., 2017b. Reducing the uncertainty of parameters controlling seasonal carbon and water fluxes in Chinese forests and its implication for simulated climate sensitivities. Global Biogeochem. Cycles 31 (8), 1344–1366.
Liu, X., Chen, B., 2000. Climatic warming in the Tibetan Plateau during recent decades. Int. J. Climatol. 20 (14), 1729–1742.
Lu, N., Wilske, B., Ni, J., John, R., Chen, J., 2009. Climate change in Inner Mongolia from 1955 to 2005-trends at regional biome and local scales. Environ. Res. Lett. 4 (4) 45006–45006.
Lu, X., Wang, Y.-P., Ziehn, T., Dai, Y., 2013. An efficient method for global parameter sensitivity analysis and its applications to the Australian community land surface model (CABLE). Agric. Forest Meteorol. 182–183, 292–303. http://dx.doi.org/10.1016/j.agrformet.2013.04.003.
Luo, Y., Wan, S., Hui, D., Wallace, L.L., 2001. Acclimatization of soil respiration to warming in a tall grass prairie. Nature 413, 622–625.
Niu, S., Li, Z., Xia, J., Han, Y., Wu, M., Wan, S., 2008a. Climatic warming changes plant photosynthesis and its temperature dependence in a temperate steppe of northern China. Environ. Exp. Bot. 63 (1–3), 91–101. http://dx.doi.org/10.1016/j.envexpbot.2007.10.016.
Niu, S., Wu, M., Han, Y., Xia, J., Li, L., Wan, S., 2008b. Water-mediated responses of ecosystem carbon fluxes to climatic change in a temperate steppe. New Phytol. 177 (1), 209–219.
Niu, S., Xing, X., Zhang, Z., Xia, J., Zhou, X., Song, B., Linghao, L.I., Wan, S., 2011. Water-use efficiency in response to climate change: from leaf to ecosystem in a temperate steppe. Global Change Biol. 17 (2), 1073–1082.
Niu, S., et al., 2012. Thermal optimality of net ecosystem exchange of carbon dioxide and underlying mechanisms. New Phytol. 194 (3), 775–783.
Peng, S., Piao, S., Shen, Z., Ciais, P., Sun, Z., Chen, S., Bacour, C., Peylin, P., Chen, A., 2013. Precipitation amount, seasonality and frequency regulate carbon cycling of a semi-arid grassland ecosystem in Inner Mongolia, China: a modeling analysis. Agric. For. Meteorol. s178-179 (4), 46–55.
Peng, F., You, Q., Xu, M., Guo, J., Wang, T., Xue, X., 2014. Effects of warming and clipping on ecosystem carbo fluxes across two hydrologically constrating years in an alpine meadow of the Qinghai-Tibetan Plateau. PLoS One 9 (10), e109319. http://dx.doi.org/10.1371/journal.pone.0109319.
Peng, S.S., et al., 2015. Benchmarking the seasonal cycle of CO_2 fluxes simulated by terrestrial ecosystem models. Global Biogeochem. Cycles 29. http://dx.doi.org/10.1002/2014GB004931.
Piao, S., Mohammat, A., Fang, J., Cai, Q., Feng, J., 2006. NDVI-based increase in growth of temperate grasslands and its responses to climate changes in China. Global Environ. Change 16 (4), 340–348.
Piao, S., et al., 2010. Forest annual carbon cost: a global-scale analysis of autotrophic respiration. Ecology 91 (3), 652–661.
Piao, S., Tan, K., Nan, H., Ciais, P., Fang, J., Wang, T., Vuichard, N., Zhu, B., 2012. Impacts of climate and CO_2 changes on the vegetation growth and carbon balance of Qinghai-Tibetan grasslands over the past five decades. Global Planet. Change 98–99 (6), 73–80.
Piao, S.L., et al., 2013. Evaluation of terrestrial carbon cycle models for their response to climate variability and to CO_2 trends. Global Change Biol. 19 (7), 2117–2132.
Reichstein, M., et al., 2005. On the separation of net ecosystem exchange into assimilation and ecosystem respiration: review and improved algorithm. Global Change Biol. 11 (9), 1424–1439. http://dx.doi.org/10.1111/j.1365-2486.2005.001002.x.
Santaren, D., Peylin, P., Bacour, C., Ciais, P., Longdoz, B., 2013. Ecosystem model optimization using in situ flux observations: benefit of Monte Carlo versus variational schemes and analyses of the year-to-year model performances. Biogeosci. Discuss. 10 (11), 18009–18064.
Schwalm, C.R., et al., 2010. Assimilation exceeds respiration sensitivity to drought: a FLUXNET synthesis. Global Change Biol. 16, 657–670.
Shangguan, W., Dai, Y., Duan, Q., Liu, B., Yuan, H., 2014. A global soil data set for earth system modeling. J. Adv. Model. Earth Syst. 6 (1), 249–263.
Shen, M., Yang, T., Chen, J., Zhu, X., Zheng, Y., 2011. Influences of temperature and precipitation before the growing season on spring phenology in grasslands of the central and eastern Qinghai-Tibetan Plateau. Agric. Forest Meteorol. 151 (2011), 1711–1722.
Shen, H.H., Wang, S.P., Tang, Y.H., 2013. Grazing alters warming effects on leaf photosynthesis and respiration in Gentiana straminea an alpine forb species. J. Plant Ecol. 6 (5), 418–427.
Shen, M., et al., 2015a. Evaporative cooling over the Tibetan Plateau induced by vegetation growth. Proc. Natl. Acad. Sci. 112 (30), 9299–9304.
Shen, M., Piao, S., Cong, N., Zhang, G., Janssens, I., 2015b. Precipitation impacts on vegetation spring phenology on the Tibetan Plateau. Global Change Biol. 21 (10), 3647–3656. http://dx.doi.org/10.1111/gcb.12961.
Shen, M., Piao, S., Chen, X., Shuai, A., Fu, Y.H., Wang, S., Nan, C., Janssens, I.A., 2016. Strong impacts of daily minimum temperature on the green-up date and summer greenness of the Tibetan Plateau. Global Change Biol. 22 (9), 3057–3066.
Song, B., Niu, S.L., Wan, S.Q., 2016. Precipitation regulates plant gas exchange and its long-term response to climate change in a temperate grassland. J. Plant Ecol. 9 (5), 531–541.
Tong, W.W., Zhang, A.Q., 2003. The relation between the Tibetan winter snow and the Asian summer monsoon and rainfall: an observational investigation. J. Clim. 16, 2038–2051.
Wagle, P., et al., 2015. Biophysical controls on carbon and water vapor fluxes across a grassland climatic gradient in the United States. Agric. For. Meteorol. 214–215, 293–305.
Wan, S.Q., et al., 2009. Photosynthetic overcompensation under nocturnal warming enhances grassland carbon sequestration. Ecology 90 (10), 2700–2710.
Wang, B., Bao, Q., Hoskins, B., Wu, G., Liu, Y., 2008a. Tibetan plateau warming and precipitation changes in east asia. Geophys. Res. Lett. 35 (14), 63–72.
Wang, Y., Zhou, G., Wang, Y., 2008b. Environmental effects on net ecosystem CO2 exchange at half-hour and month scales over Stipa krylovii steppe in northern China. Agric. Forest Meteorol. 148 (5), 714–722. http://dx.doi.org/10.1016/j.agrformet.2008.01.013.
Wang, H.S., Jia, G.S., Feng, J.M., Zhao, T.B., Ma, Z.G., 2010. Modeling gross primary production by integrating satellite data and coordinated flux measurements in arid and semi-arid China. Atmos. Oceanic Sci. Lett. 3 (1), 7–13. http://dx.doi.org/10.1080/16742834.2010.11446842.
Wang, T., et al., 2012. State-dependent errors in a land surface model across biomes inferred from eddy covariance observations on multiple timescales. Ecol. Modell. 246, 11–25. http://dx.doi.org/10.1016/j.ecolmodel.2012.07.017.
Xia, J.Y., et al., 2015. Joint control of terrestrial gross primary productivity by plant phenology and physiology. Proc. Natl. Acad. Sci. 112 (9), 2788–2793.
Xu, L., Zhang, X., Shi, P., Yu, G., Sun, X., 2005. Net ecosystem carbon dioxide exchange of alpine meadow in the Tibetan Plateau from August to October. Acta Ecol. Sin. 25 (8), 1948–1952.
Yang, Z.L., et al., 2016. Nighttime warming enhances drought resistance of plant communities in a temperate steppe. Sci. Rep. 6 (2326), 7.
Yang, K., 2017. Observed Regional Climate Change in Tibet over the Last Decades. Oxford Research Encyclopedia of Climate Science, pp. 1–41. http://dx.doi.org/10.1093/acrefore/9780190228620.013.587.
Yin, X., Struik, P.C., 2009. C_3 and C_4 photosynthesis models: an overview from the perspective of crop modelling. NJAS-Wageningen J. Life Sci. 57, 27–38.
Yuan, W.P., et al., 2007. Deriving a light use efficiency model from eddy covariance flux data for predicting daily gross primary production across biomes. Agric. Forest Meteorol. 142 (3–4), 189–207.
Zhang, B., Cao, J., Bai, Y., Zhou, X., Ning, Z., Yang, S., Hu, L., 2013. Effects of rainfall amount and frequency on vegetation growth in a Tibetan alpine meadow. Clim. Change 118, 197–212.
Zhang, Y., et al., 2014. Spatial and temporal variability in the net primary production of alpine grassland on the Tibetan Plateau since 1982. J. Geog. Sci. 24 (2), 269–287.